Rare Earth Metal Boron Carbide MBC Compounds Containing Monodimensional Branched Zigzag Chains of Non-Metal Atoms: Theoretical Aspects

Fabrice Wiitkar, Samia Kahlal, Jean-François Halet,* and Jean-Yves Saillard*

Laboratoire de Chimie du Solide et Inorganique Moléculaire, URA CNRS 1495, Université de Rennes I, 35042 Rennes, France

Josef Bauer

Laboratoire de Chimie du Solide et Inorganique Moléculaire, URA CNRS 1495, Institut National des Sciences Appliquées, 35043 Rennes, France

Peter Rogl

Institut für Physikalische Chemie, Universität Wien, Währingerstrasse 42, A-1090 Wien, Austria

Received September 30, 1994[⊗]

The electronic structure and bonding properties of the rare earth metal boron carbide materials containing boron−carbon zigzag chains are analyzed and compared by means of extended Hückel tight-binding calculations. The results show that an ionic picture between the metallic framework, and the boron−carbon chains can easily explain the arrangement, regular or distorted, of the latter. Thus, a formal charge of 3− per BC unit accounts for the regular chains encountered in YBC and UBC. With a formal charge greater than 3− per BC unit, distorted chains due to a Peierls instability are expected as in $UB_{0.78}C_{1.22}$, ThBC, and $Th_3B_2C_3$. In the three-dimensional materials, the metal−non-metal bonding occurs primarily through electron donation from the anionic sublattice toward the metallic elements. Metallic behavior is expected for all the materials. The structural arrangement in the different MBC compounds is discussed.

Introduction

The combination of boron and carbon with rare earth metals[1] leads to the formation of materials having interesting physical and structural properties. In these compounds, of formula $M_xB_yC_z$, the non-metal atoms form either two-dimensional (2-D) networks, monodimensional (1-D) zigzag chains, or finite linear units of various length.[2] The dimensionality of the boron−carbon sublattice is related to the averaged valence electron count (VEC) per light atom (B or C).[2] This VEC is calculated assuming a simple ionic bonding scheme between the metal atoms and the B/C net and a fully oxidized metal M^{n+} (*i.e.* $n = 3$ generally, or possibly 4 as for Ce, Th, or U, for example), in the following way: $VEC = (nx + 3y + 4z)/(y + z)$.

Compounds in which 2-D B/C nets are present have the lowest values of VEC, which are between 4.1 and 4.7.[2] The formal addition of electrons to these structures corresponds to the occupation of antibonding boron−carbon states, inducing bond breaking and consequently a loss of connectivity between the boron and carbon atoms. It follows that the materials containing finite units of non-metal atoms are more electron-rich, with VEC values spreading over the range 4.9−5.7. The class of materials in which the carbon and boron atoms form 1-D systems, corresponds to intermediate values of VEC of around 5.

This paper deals with the study of the electronic structure of this latter family. The calculations were performed using extended Hückel tight-binding calculations (see the Appendix for the computational details). This work is part of a general theoretical and topological understanding of the structures and properties of these ceramics that we have recently undertaken.[2−4]

Description of the Structures

Table 1 summarizes some relevant data for the different rare earth boron carbides containing 1-D boron−carbon chains, which have been characterized by X-ray or neutron diffraction techniques.

Three different structural types corresponding to the MBC composition have been reported thus far, namely YBC,[5] UBC,[9,10] and ThBC.[13] They are represented in Figures 1−3,

[⊗] Abstract published in *Advance ACS Abstracts,* February 1, 1995.

(1) Throughout this paper, the word "rare earth" refers to the elements Sc, Y, lanthanides, and actinides.

(2) Wiitkar, F.; Kahlal, S.; Halet, J.-F.; Saillard, J.-Y.; Bauer, J.; Rogl, P. *J. Am. Chem. Soc.* **1994**, *116*, 251.

(3) Halet, J.-F.; Saillard, J.-Y.; Bauer, J. *J. Less-Common Met.* **1990**, *158*, 239.

(4) Wiitkar, F.; Halet, J.-F.; Saillard, J.-Y.; Rogl, P.; Bauer, J. *Inorg. Chem.* **1994**, *33*, 1297.

(5) Bauer, J.; Nowotny, H. *Monatsh. Chem.* **1971**, *102*, 1129.

(6) Bauer, J.; Debuigne, J. *C. R. Acad. Sci. (Paris), Sér. C* **1972**, *274*, 1271.

(7) Bauer, J.; Venneguès, P.; Vergneau J. L. *J. Less-Common Met.* **1985**, *110*, 295.

(8) Bauer, J. *Proceedings of the VIIth International Conference on Solid Compounds of Transition Elements*; Vienna: Austria, April 1985.

(9) Toth, L.; Nowotny, H.; Benesovsky, F.; Rudy, E. *Monatsh. Chem.* **1961**, *92*, 794.

(10) Rogl, P.; Rupp, B.; Felner, I.; Fischer, P. *J. Solid State Chem.* **1993**, *104*, 377.

(11) Klesnar, H.; Rogl, P. *AIP Proceedings 231 on Boron Rich Solids*; Emin, D., Ed.; Albuquerque, NM, 1991; p 414.

(12) (a) Rogl, P.; Beauvy, M.; Larroque, J. *Proceedings of the XIXème Journées des Actinides*; Madonna di Campiglio: Italy, 1989; p 95. (b) Rogl, P. In *The Physics and Chemistry of Carbides, Nitrides and Borides*; Freer, R., Ed.; Kluwer Academic Publishers: Dodrecht, Netherlands, 1990; p 269.

(13) Rogl, P. *J. Nucl. Mater.* **1978**, *73*, 198.

0020-1669/95/1334-1248$09.00/0

Table 1. Rare Earth Boron Carbide and Related Compounds Containing 1-D Zigzag Chains of Main-Group Atoms, Characterized by X-ray or Neutron Diffraction

structural type	compound[a]	VEC[b] $n=3$	VEC[b] $n=4$	d_{B-B} (Å)	d_{B-C} (Å)	ref
YBC (*Cmmm*)	YBC	5.00		2.00	1.64	5
	DyBC	5.00				6
	HoBC	5.00				7
	ErBC	5.00				8
UBC (*Cmcm*)	UBC	5.00	5.50	1.90	1.52	9, 10
	$UB_{0.78}C_{1.22}$	5.11	5.61	1.89	1.53	10
	$UB_{0.78}C_{1.22}$[c]	5.11	5.61	1.71/2.04	1.55	10
	UBN	5.50	6.00	1.89	1.50[d]	11
	NpBC	5.00	5.50			12
	PuBC	5.00	5.50			12
ThBC (*P*4₁22)	ThBC		5.50	1.77/2.47	1.54	13
$Th_3B_2C_3$ (*P*2/*m*)	$Th_3B_2C_3$		5.50	1.77/2.30	1.55	14

[a] Characterized by X-ray diffraction, unless otherwise specified. [b] Averaged valence electron count per light atom; The value given for $Th_3B_2C_3$ assumes the formal topochemical separation: 2ThC + ThBC. [c] Characterized by neutron diffraction as having *C*2/*m* symmetry. [d] d_{B-N}.

respectively. In all of them, the metal atoms form trigonal prisms which condense along one direction through square faces, making infinite channels. The boron atoms occupy the middle of the metallic prisms and form zigzag chains, to which the carbon atoms are tethered (**1**). Boron atoms are then surrounded by six metal atoms, two boron congeners and one carbon atom. The assemblage of motif **1** in a second dimension by sharing metallic triangular faces makes 2-D MBC slabs (**2**). These slabs can stack in several ways, leading to the different structural types given in Table 1.

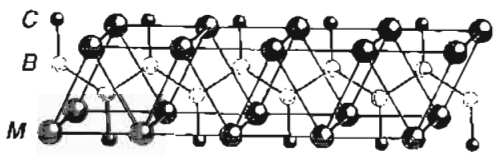

1

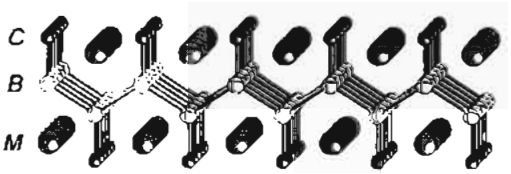

2

In the YBC material, the zigzag boron chains are regular with B−B and B−C distances of 2.00 and 1.64 Å, respectively.[5] Though the crystal structure of YBC is not very accurate, these B−B and B−C separations can be considered as lying in the range of usual single bonds and double bonds, respectively. The other contacts in the slabs are 2.55 Å for Y−C, between 2.69 and 2.78 Å for Y−B and from 3.39 to 3.63 Å for Y−Y. The slabs stack in such a way that they are symmetrically facing each other, leading to Y−Y (3.70 Å) and C···C (2.49 Å) interslab contacts (see Figure 1). This corresponds to a translation of $^1/_2a$ (parallel to the zigzag chains) + $^1/_2b$. Note that a structural relationship exists between the YBC and AlB_2 phases.[15] Such a stacking leads to carbon atoms lying in highly distorted octahedra made of four coplanar metal atoms and two capping boron and carbon atoms (see Figure 1). The long C···C interslab separations are somewhat puzzling. They are far

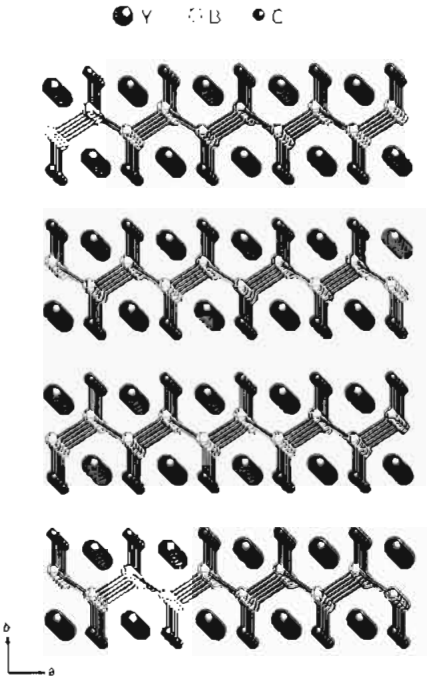

Figure 1. Crystal structure of YBC.

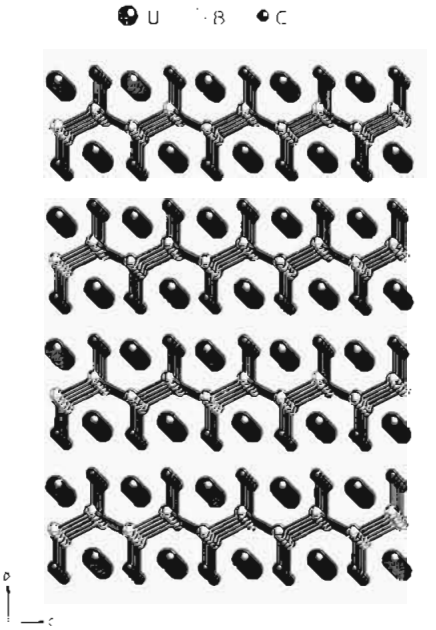

Figure 2. Crystal structure of UBC.

beyond usual C−C single bonds (1.54 Å), but much shorter than the van der Waals separations (3.70 Å as in graphite). We will come back to this point later.

In UBC the slabs stack again along the *b* axis, but this time with a translation of $^1/_2a$ perpendicular to the zigzag chains, leading to the formation of U−C contacts only (see Figure 2).[9,10] These rather short U−C distances of 2.34 Å ensure the 3-D character of the material, leading to a $[U_5B]$ octahedral environment for the carbon atoms in contrast with the $[Y_4BC]$ one in YBC. The powder X-ray and neutron crystal structure determinations of UBC and its related nitrogen-containing phases deserve some comments. The earliest study of UBC performed with X-ray techniques on powder, indicates the centrosymmetric space group *Cmcm* (see Table 1), in which all the B−B distances are symmetrically related and consequently equal ($d = d' = 1.88$ Å).[9] More recently, a single crystal X-ray determination carried out on the stoichiometric UBC and

(14) Rogl, P. *J. Nucl. Mater.* **1979**, *79*, 154.
(15) Rogl, P. *J. Nucl. Mater.* **1979**, *80*, 187.

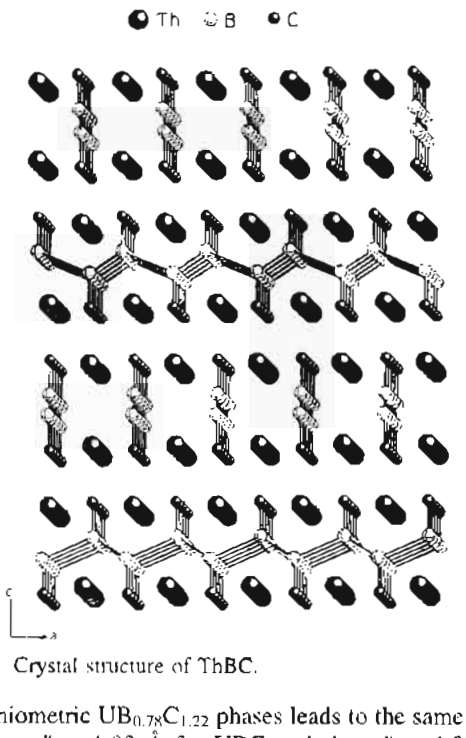

Figure 3. Crystal structure of ThBC.

nonstoichiometric $UB_{0.78}C_{1.22}$ phases leads to the same conclusions ($d = d' = 1.90$ Å for UBC and $d = d' = 1.89$ Å for $UB_{0.78}C_{1.22}$).[10] However, a powder neutron diffraction study of the latter indicates the noncentrosymmetric space group $C2/m$, in which the boron atom chains present alternating short and long bond distances ($d = 1.71$ Å; $d' = 2.04$ Å).[10] Since neutron diffraction techniques generally give more accurate positions for the light atoms in presence of heavy elements, such a result questions the existence of the regular boron chains in UBC, as well as in the related UBN compound.[11] In other words, is a B−B bond alternation also present in UBC and UBN? On the other hand, it seems that there is no ambiguity for the B−C separations. Distances ranging between 1.52 and 1.55 Å, suggesting some double bond character, are measured in the different studies.[9,10] U−B and U−C separations are *ca.* 2.75 and 2.40 Å, respectively. U−U contacts from 3.35 to 3.72 Å were measured.

The third structural type of stoichiometry MBC (ThBC) can be deduced from that of UBC by a double shift operation ($^1/_2a + {}^1/_2c$; see Figures 2 and 3).[13] Such a double shift does not change the environment of the carbon atoms and the nature of the interslab contacts which remain of the same type as in UBC (Th−C = 2.51 Å). The major difference with YBC and UBC concerns the slab itself. It is noteworthy that the powder X-ray study of ThBC indicates a strong alternation between the B−B contacts ($d = 1.77$ Å; $d' = 2.47$ Å).[13] The existence of a significant bonding contact for the latter is therefore questionable. The other contacts inside the slabs are *ca.* 2.96 Å for Th−B and range between 2.62 and 2.72 Å and between 3.76 and 3.86 Å for Th−C and Th−Th, respectively.

The same feature, i.e. the presence of distorted boron zigzag chains, is observed in the ThBC slabs present in $Th_3B_2C_3$ ($d = 1.77$ Å; $d' = 2.30$ Å).[14] Indeed, the crystal structure of $Th_3B_2C_3$ can be derived from that of UBC by intercalating ThC layers (NaCl type) between the ThBC slabs (see Figure 4) and may be considered as the topochemical sum of 2ThBC + ThC.[14] The isolated carbon atoms of the ThC layers are then surrounded by distorted metal octahedra (Th−C = 2.54−2.67 Å). As in UBC and ThBC, the carbon atoms bound to the boron atoms of the chains have an octahedral [Th_5B] environment (Th−C = 2.63−2.68 Å). The averaged Th−B distances are 2.93 Å and the Th−Th contacts range between 3.70 and 4.08 Å, slightly

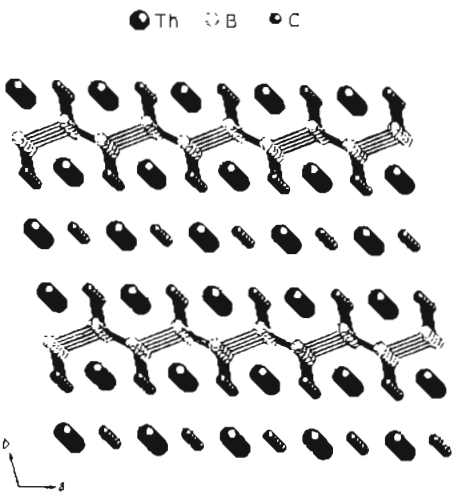

Figure 4. Crystal structure of $Th_3B_2C_3$.

longer than the corresponding ones measured in ThBC. Note that although the ionic radii of the Th and U metal atoms are fairly comparable,[16] the M−M, M−B, and M−C separations are noticeably longer in the ThBC and $Th_3B_2C_3$ species than in the UBC one. This suggests stronger covalent bonding in the latter (see below).

Electronic Structure of the MBC (M = Y, U, Th) and $Th_3B_2C_3$ Phases

We first tackle the B−B and B−C bonding analysis in the zigzag chains within the framework of a simple ionic bonding scheme between the metal and the non-metal sublattices. Indeed, this simple approach has been proven to be extremely helpful to rationalize the structural arrangement and the atomic connectivity of the non-metal sublattice in the rare earth boron carbides.[2-4,17] In a second step, we analyze the metal−non-metal interactions inside a slab. Finally, the different interslab interactions are considered.

(a) The 1-D Branched Chains of Boron and Carbon. Assuming a purely ionic bonding mode between the metal atoms and the non-metal 1-D chains, the first question which arises concerns the ionic charges. The oxidation state for yttrium is 3+ ($4d^0\ 5s^0$). The most common oxidation state for actinides is also 3+. However, thorium makes an exception with a usual oxidation state of 4+ ($5f^06d^07s^0$).[16] In the case of uranium, both oxidation states of 3+ ($5f^36d^07s^0$) and 4+ ($5f^26d^07s^0$) are common.[16] Therefore, we start our analysis by first looking at the electronic structure of an isolated $[(BC)^{3-}]_\infty$ and $[(BC)^{4-}]_\infty$ regular ($d = d'$) zigzag chain. This regular chain presents a 2_1 screw axis with a unit cell containing two BC repeating units.

The π MO diagram associated with the B_2C_2 unit cell is shown in Figure 5a. It is related to that of *trans*-butadiene, with some changes coming from the electronegativity difference between boron and carbon.[18] The bonding π_1 and π_2 levels are preferentially localized on the more electronegative carbon atoms, while the antibonding π_3 and π_4 levels are mainly localized on the less electronegative boron atoms. The band structure of the regular chain is shown in Figure 5b, with the π-bands in bold. The screw axis leads to band degeneracy at X ($k = \pi/a$).[19] The two lowest π-bands, which derive primarily from the π_1 and π_2 levels of the unit cell contents are rather

(16) See for example: Greenwood, N. N.; Earnshaw, A. *Chemistry of the Elements*; Pergamon Press: Oxford, England, 1984.
(17) Burdett, J. K.; Canadell, E.; Hughbanks, T. *J. Am. Chem. Soc.* **1986**, *108*, 3971.
(18) Pauling, L. *The Nature of the Chemical Bond*, Cornell University Press: Ithaca, NY, 1960.

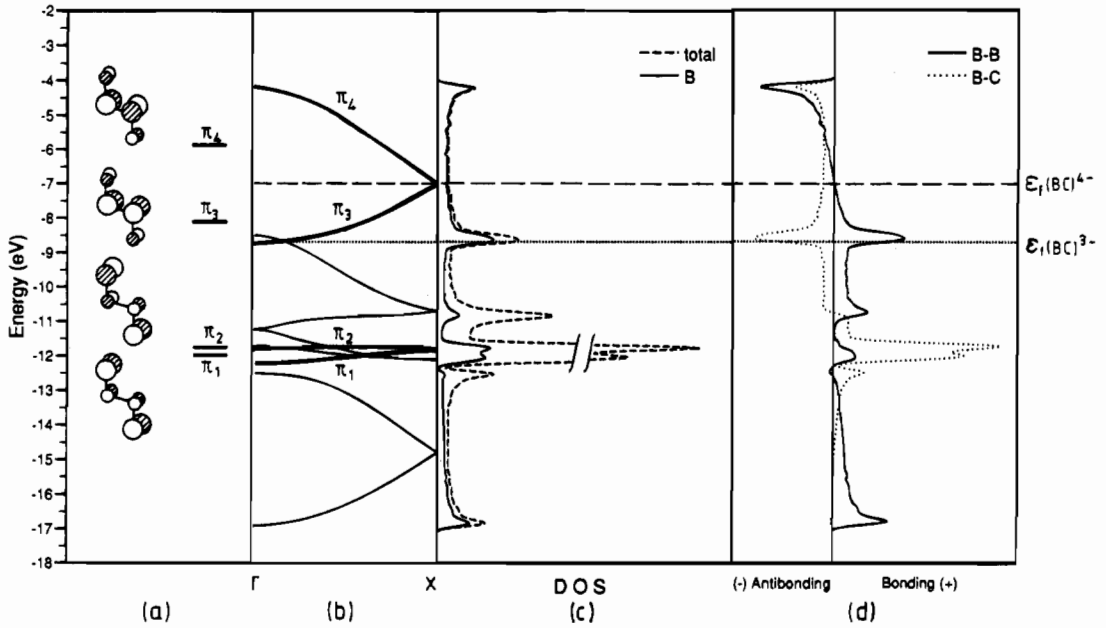

Figure 5. (a) π MO diagram for the B_2C_2 motif contained in the unit cell of the $[BC]_\infty$ chain; (b) band structure with π-bands in bold line; (c) total density of states (dashed line) and boron contribution (solid line); (d) COOP curves of B−B (solid line) and B−C (dotted line) bonds for the regular zigzag $[BC]_\infty$ chain. The Fermi level is indicated for a charge of 3− (dotted line) and 4− (dashed line) per BC unit.

flat, due to their poor localization on the boron atoms. On the other hand, the two highest π-bands, descending from the primarily boron π_3 and π_4 levels, are more dispersed. For a charge of 3− per BC unit, the Fermi level (ϵ_F) cuts the bottom of the π_3 band. The band crossing between the bottom of the π_3 band and the top of the highest occupied σ-band could be an artifact of the extended Hückel method. It is well-known that such a method often overestimates the energy of the σ levels with respect to the π ones. It should be noted however that calculations carried out by Cui and Kertesz on polyketone ($[CO]_\infty$), a hypothetical polymer isostructural and isoelectronic to the $[(BC)^{3-}]_\infty$ chain, find a similar crossing near ϵ_F.[20] The authors conclude that such a planar structure should undergo an out-of-plane distortion (second-order Peierls instability), leading to the formation of a HOMO/LUMO gap through σ/π mixing. Indeed, their calculations favor a helical structure.[20] Kollmar and Hoffmann have obtained the same result for polyisocyanides ($[CNR]_\infty$), but they attribute the departure from planarity to nitrogen lone-pair repulsion.[21] Anyhow, whether the σ/π crossing near ϵ_F is real or not in the $[(BC)^{3-}]_\infty$ chain, we conclude that, at least in the environment of the metal cations, such a second-order Peierls instability must be too weak to induce an out-of-plane distortion. No significant departure from planarity has been observed in the different characterized MBC and $M_3B_2C_3$ materials.

The full occupation of two π-bands (π_1 and π_2) in the band structure diagram of the $[(BC)^{3-}]_\infty$ chain is consistent with the Lewis formula depicted in **3**. The two lowest occupied π-bands can be unambiguously associated with the two B−C π bonding doublets contained in the unit cell, whereas the two (almost) empty upper π-bands (π_3 and π_4) correspond to the B−C π antibonding states.

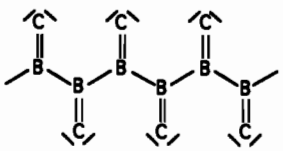

3

The density of states (DOS) of the 1-D organic $[BC]_\infty$ network is shown in Figure 5c. The overlap of the bottom of the π_3 band with the top of the highest occupied σ-band induces a large peak of DOS around ϵ_F, indicating a possible conducting behavior for the hypothetical 1-D $[(BC)^{3-}]_\infty$ chain. This peak is mainly boron in character. The variation of the B−B and B−C overlap populations with respect to the energy (COOP curves)[22] is represented in Figure 5d. For the considered electron count of 3− per BC unit, the B−B and B−C COOP curves are highly positive and largely negative above ϵ_F, respectively. This situation allows the best compromise between the B−B and B−C bond strengths in a regular $[(BC)^{3-}]_\infty$ chain.

With two more electrons per unit cell (*i.e.* a $[(BC)^{4-}]_\infty$ chain), the π_3 band becomes fully occupied, leading to a HOMO/LUMO degeneracy at the edge of the Brillouin zone X ($k = \pi/a$). This is a typical situation of a first-order Peierls instability, as in polyacetylene, for example.[19] A distorted structure, corresponding to alternation of short and long B−B bonds is thus expected. In agreement with this statement, calculations on a distorted $[(BC)^{4-}]_\infty$ chain (d = 1.82 Å and d' = 2.22 Å) show the opening of a large HOMO/LUMO gap of 1.2 eV (see Figure 6). It is noteworthy that, for this electron count, the COOP curve corresponding to the short B−B contacts (1.82 Å) changes its bonding character into an antibonding one at the Fermi level (see Figure 6c). This is a situation which is often encountered in the main-group sublattices of rare earth boron carbides.[2-4,17] Note also that the B−C overlap populations are weakened for the charge of 4- with respect to the charge of 3− (1.010 *vs* 0.772). This indicates that the stability of the B/C chain is now dominated by B−B rather than by B−C bonding.

(19) For an introduction to the electronic structure of polyacetylene, see for example: (a) Whangbo, M.-H.; Hoffmann, R.; Woodward, R. B. *Proc. R. Soc. London* **1979**, *A366*, 23. (b) Cui, C. X. Kertesz, M.; Jiang, Y. *J. Phys. Chem.* **1990**, *94*, 5172. (c) Hoffmann, R., Janiak, C.; Kollmar, C. *Macromolecules* **1991**, *24*, 3725. (d) Paloheimo, J.; von Boehm, J. *Phys. Rev.* **1993**, *B48*, 16948.

(20) Cui, C.-X.; Kertesz M. *Chem. Phys. Lett.* **1990**, *169*, 445.

(21) Kollmar, C.; Hoffmann R. *J. Am. Chem. Soc.* **1990**, *112*, 8230.

(22) (a) Hughbanks, T.; Hoffmann, R. *J. Am. Chem. Soc.* **1983**, *105*, 3528. (b) Wijeyesekara, S. D.; Hoffmann, R. *Organometallics* **1984**, *3*, 949. (c) Kertesz, M.; Hoffmann, R. *J. Am. Chem. Soc.* **1984**, *106*, 3483.

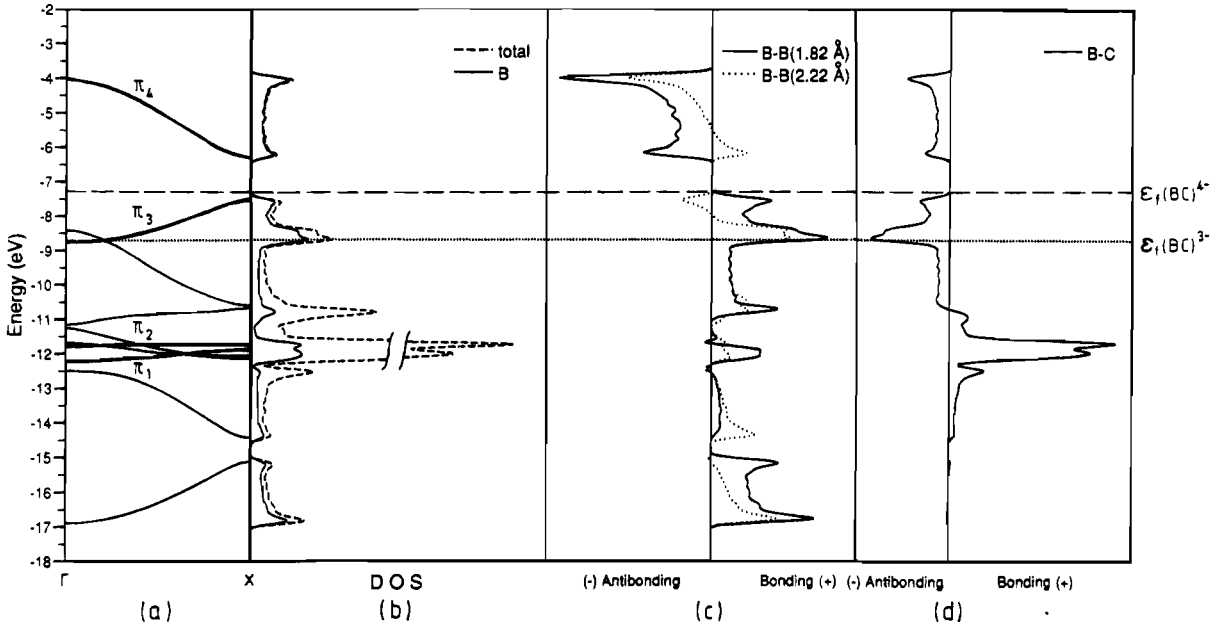

Figure 6. (a) Band structure with π-bands in bold line; (b) total density of states (dashed line) and boron contribution (solid line); (c) COOP curves of short B−B (solid line) and long B−B contacts (dotted line); (d) COOP curve of B−C bonds for the distorted zigzag $[BC]_\infty$ chain. The Fermi level is indicated for a charge of 3− (dotted line) and 4− (dashed line) per BC unit.

Table 2. Characteristics Computed with Different Electron Counts for the 1-D (BC), 2-D (MBC Slab) and 3-D (MBC) Models Containing Regular Boron−Carbon Chains

	regular chain							
	BC network		2-D MBC network		3-D YBC network		3-D UBC network	
	EN[a] = 10	EN = 11	EN = 10	EN = 11	EN = 10	EN = 11	EN = 10	EN = 11
tot. energy (eV)[b]	−144.22	−152.37	−151.01	−161.11	−150.28	−160.29	−151.48	−161.27
ϵ_F (eV)	−8.70	−7.01	−10.57	−9.64	−10.34	−9.58	−10.33	−9.27
			Overlap Populations					
B−B (2.02 Å)	0.738	0.892	0.466	0.523	0.478	0.523	0.479	0.535
B−C (1.60 Å)	1.010	0.772	0.945	0.871	0.900	0.881	0.943	0.863
M−B (2.67 Å)[c]			0.097	0.132	0.106	0.130	0.114	0.145
M−C (2.54 Å)[c]			0.308	0.315	0.321	0.326	0.230	0.244
M−M (3.50 Å)[c]			0.048	0.066	0.056	0.072	0.027	0.044
M−M[d]					−0.025	−0.009	0.018	0.009
C−C (2.50 Å)[d]					−0.022	−0.086		
M−C (2.30 Å)[d]							0.500	0.455
			Atomic Net Charges					
B	−0.06	−0.80	+0.48	+0.15	+0.43	+0.15	+0.39	+0.09
C	−2.94	−3.20	−1.70	−1.87	−1.56	−1.87	−1.47	−1.73
M			+1.22	+1.72	+1.13	+1.72	+1.08	+1.64

[a] EN = electron number per motif. The numbers of 10 and 11 correspond to a metal valence electron count of 3 and 4, respectively. [b] Per motif. [c] Intraslab contact. [d] Interslab contact.

As expected from the results discussed above, the distorted $[(BC)^{4-}]_\infty$ chain is slightly favored over the regular chain. For the $[(BC)^{3-}]_\infty$ chain on the other hand, it is the regular one which is preferred (see Tables 2 and 3). However, the energy differences (0.04 and 0.05 eV per $(BC)^{4-}$ and (BC)3− motif, respectively) appear to be rather weak. When only the π energy is considered, the distorted chain is now preferred by 0.13 eV per BC motif for $[(BC)^{4-}]_\infty$. This is almost exclusively due to the stabilization of the π_3 band, which is mainly localized on the B atoms, since the π energies for the regular and the distorted chain are nearly equal for $[(BC)^{3-}]_\infty$ (see Figures 5 and 6). Clearly, EH calculations do not reproduce correctly the σ energy in the models we considered. A detailed analysis of our computational results indicate that the major reason comes from an overestimation of σ-type second-neighbor interactions.

With three π electron pairs per unit cell, the Lewis formula shown in **4** fits nicely with the band structure illustrated in Figure 6a. It accounts for the shortening of the B−B bonds (partial B−B double bond character) and the lengthening of the B−C bonds, due to the occupation of the π_3 band, which is π B−B bonding and π B−C antibonding.

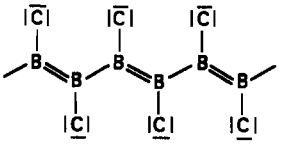

4

Other mesomeric Lewis formulas can also be considered for a charge of 4− per BC entity such as those shown in **5** and **6**, which possess a π-electron count in agreement with the band structure represented in Figure 6a. A partial B−C double bond character is kept, in agreement with the fact that the B−C antibonding π_4 band is vacant. However, since they suppose a regular boron chain, their weight with respect to that of **4** must

Table 3. Characteristics Computed with Different Electron Counts for the 1-D (BC), 2-D (MBC Slab) and 3-D (MBC) Materials Containing Distorted Boron−Carbon Chains (The Experimental Structure Was Used for $Th_3B_2C_3$)

	distorted chain							
	BC network		2-D MBC network		3-D ThBC network		3-D $Th_3B_2C_3$ network	
	EN[a] = 10	EN = 11	EN = 10	EN = 11	EN = 10	EN = 11	EN = 10	EN = 11
tot. energy (eV)[e]	−144.17	−152.41	−151.04	−161.13	−151.45	−161.30	−411.05	−441.26
ϵ_F (eV)	−8.71	−7.57	−10.56	−9.57	−10.42	−9.32	−10.94	−9.58
				Overlap Populations				
B−B (1.82 Å)	0.875	1.144	0.617	0.686	0.630	0.705	0.653	0.790
B−B (2.22 Å)	0.599	0.671	0.333	0.380	0.339	0.386	0.291	0.373
B−C (1.60 Å)	1.008	0.771	0.944	0.870	0.942	0.862	1.029	0.919
M−B[b]			0.099	0.136	0.110	0.140	0.064	0.103
M−C (2.62 Å)[b]			0.311	0.318	0.214	0.225	0.234	0.244
M−M (3.50 Å)[b]			0.048	0.062	0.026	0.040	0.028	0.086
M−M (3.88 Å)[c]					0.018	0.009	0.040	0.047
M−C (2.4−2.46 Å)[c]					0.328	0.328	0.403	0.427
M−C (octa)[d]							0.338	0.332
				Atomic Net Charges				
B	−0.06	−0.80	+0.47	+0.14	+0.41	+0.08	+0.56	+0.07
C	−2.94	−3.20	−1.69	−1.86	−1.50	−1.73	−1.94	−2.04
M			+1.22	+1.72	+1.09	+1.65	+0.83	+1.58
M[d]							+1.44	+1.84
C(octa)[d]							−1.45	−1.68

[a] EN = electron number per motif. The numbers of 10 and 11 correspond to a metal valence electron count of 3 and 4, respectively. [b] Intraslab contact. [c] Interslab contact. [d] In $Th_3B_2C_3$. [e] Per motif.

be weaker. As formula **4**, the one sketched in **7** accounts for the alternation of short and long B−B contacts. The $(B_2C_2)^{8-}$ units are in turn isolated from each other. At first sight, this is in agreement with the long B−B separations measured in ThBC ($d' = 2.47$ Å).[13] Nevertheless, **7** possesses a number of π (and σ) electrons different from that of **4** (2 *vs* 3 per (BC) motif). Therefore, **7** must be considered as an alternative isomeric form of **4**, not as a mesomeric one. It is noteworthy that this $(B_2C_2)^{8-}$ unit is isoelectronic to the *trans*-isomer of N_2O_2, which is known to be a rather unstable dimer of nitric oxide.[23] EH calculations performed on a $(B_2C_2)^{8-}$ entity taken from ThBC, show no HOMO/LUMO gap and a level ordering in disagreement with the number of σ and π electrons pairs required by **7**. It turns out that one of the σ-type nonbonding levels associated with the boron lone pairs, which should be occupied, lies above the B−B antibonding π_3 level, which should be vacant. Consequently, the description of the isolated 1-D distorted $[(BC)^{4-}]_\infty$ chains present in ThBC as being the assemblage of independent $(B_2C_2)^{8-}$ units should be ruled out. This is supported by calculations performed on this type of distorted chain such as the one present in ThBC where $d = 1.77$ Å and $d' = 2.47$ Å. They still show rather important overlap populations for d' (0.507 *vs* 1.208 for d), reflecting a significant B−B bonding between the $(B_2C_2)^{8-}$ entities. Nevertheless, the mixing of the electronic configurations **4** and **7**, symmetry forbidden in the 1-D $[(BC)^{4-}]_\infty$ chain, is allowed in the real 3-D MBC material. Indeed, the results on the 3-D ThBC model (vide infra) based on the analysis of the occupation of the frontier orbitals of the (B_2C_2) units indicate some participation of **7** in the ground state (0.86 and 0.48 electron in π_3 and in the boron σ-type MO lying above π_3, respectively). To some extent, this mixing of the electronic configurations **4** and **7** in the solid could partly be responsible for the long bonds, which are observed in ThBC and $Th_3B_2C_3$.[13,14]

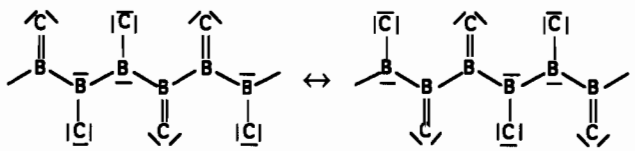

5

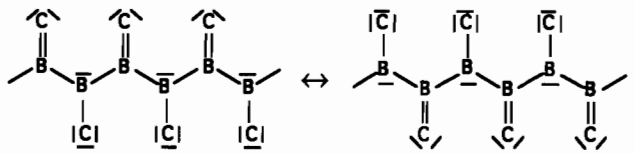

6

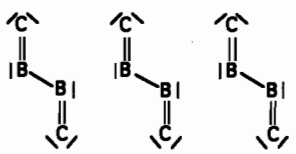

7

Considering a purely ionic bonding scheme between the nonmetal and metal atoms, the simple analysis of the electronic structure of the 1-D boron−carbon chains allows us to understand why these chains are regular in YBC (Y^{3+}, $(BC)^{3-}$), and distorted with alternatively short and long B−B contacts in ThBC (Th^{4+}, $(BC)^{4-}$) and $Th_3B_2C_3$ (Th^{4+}, C^{4-}, $(BC)^{4-}$). UBC and its related compounds can be rationalized in the same way, assuming that uranium is trivalent. Therefore the stoichiometric UBC phase (U^{3+}, $(BC)^{3-}$) should present regular chains, as observed experimentally.[9,10] On the contrary, the $UB_{0.78}C_{1.22}$ (U^{3+}, $(BC)^{3.22-}$ and UBN (U^{3+}, $(BN)^{3-}$) phases, richer in electrons, should present slightly and highly distorted chains, respectively. An accurate powder neutron diffraction study of $UB_{0.78}C_{1.22}$ reveals a zigzag boron chain which is slightly distorted.[10] On the other hand, the boron−nitrogen chain in UBN would be regular according to a powder X-ray experiment.[11] If it is the case, ionic formulas such as (U^{2+}, $(BN)^{2-}$) and (U^{4+}, $(BN)^{4-}$), would account for the absence of distortion.

(23) See for example: (a) Bardo, R. D. *J. Phys. Chem.* **1982**, *86*, 4658. (b) Ritchie, J. P. *J. Phys. Chem.* **1983**, *87*, 2466. (c) Nour, E. M.; Chen, L.-H.; Strube, M. M.; Laane, J. *J. Phys. Chem.* **1984**, *88*, 756. (d) Lee, T. J.; Rice, J. E.; Scuseria, G. E.; Schaefer III, H. F. *Theor. Chim. Acta* **1989**, *75*, 81. (e) Jones, W. H. *J. Phys. Chem.* **1991**, *95*, 2588. (f) Jones, W. H. *J. Phys. Chem.* **1992**, *96*, 594. (g) Jones, W. H. *J. Phys. Chem.* **1992**, *96*, 5184. (h) Howard, B. J.; McKellar, A. R. W. *Mol. Phys.* **1993**, *78*, 55.

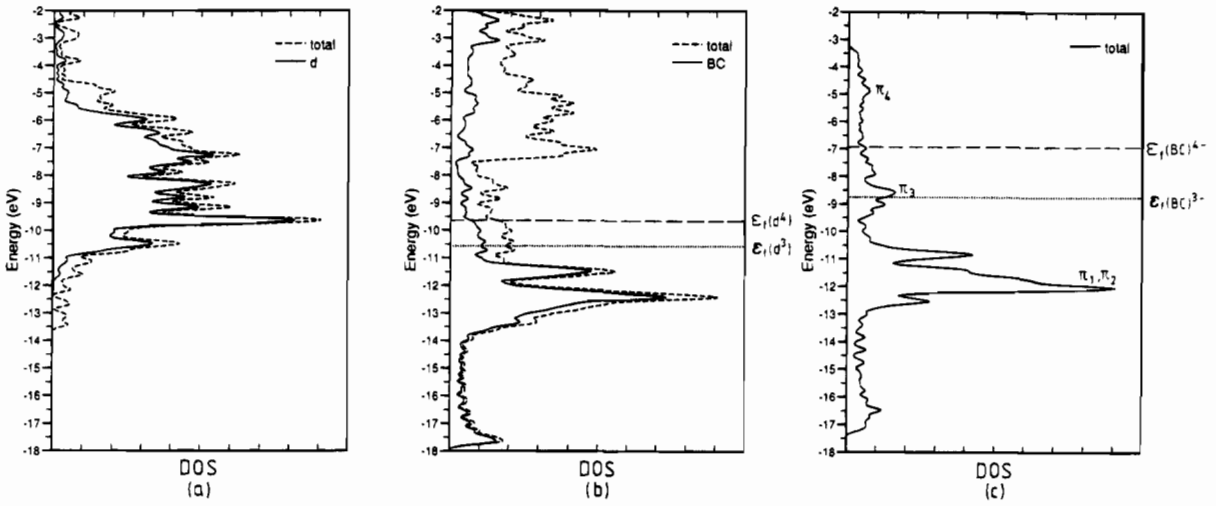

Figure 7. (a) Total DOS (dashed line) and metallic d contribution (solid line) for the 2-D metallic sublattice before interaction. (b) Total DOS (dashed line), total boron + carbon contribution (solid line) for the 2-D slab MBC. (c) Total DOS for the boron−carbon sublattice before interaction. The Fermi level is indicated for a valence electron count of 3 (dotted line) and 4 (dashed line) per metal.

The former appears possible, but the latter, which corresponds to B−N single bonds, is not consistent with the experimental distances (see Table 1). Experimental work (neutron diffraction) is in progress in order to obtain the structure of UBN with a better accuracy.

(b) Effect of the Metallic Environment on the Boron−Carbon Chains: Electronic Structure of the 2-D MBC Slab. As stated previously, the repeating motif common to all the MBC compounds is the 2-D MBC slab shown in **2**. We have therefore decided to look first at the effect of the metallic environment on the regular and distorted B/C chains with the analysis of the electronic structure of an MBC slab. In order to allow a comparison of the different computed data, calculations have been carried out on a slab where certain atomic separations have been idealized (see the Appendix).

The DOS of the metallic and boron−carbon sublattices ($d = d' = 2.02$ Å) are shown on the left-hand side and the right-hand side of Figure 7, respectively. Since the boron−carbon chains are far from each other (3.50 Å), the total DOS of the boron−carbon network is comparable to that shown in Figure 5c. The DOS of the metallic slab spreads over 10 eV, with a broad peak around −8.0 eV due to the d orbitals. Such a broadening reflects some significant metal−metal interactions. A look at the DOS after interaction, illustrated in the center of Figure 7, clearly indicates that the bonding between the two sublattices is not simply ionic, but significantly covalent. The boron−carbon DOS is now more dispersed. The important B/C peak centered at −12 eV before interaction, is broadened and stabilized by more than 1 eV. The upper peaks due to the B/C π_3 and π_4 band are pushed higher in energy. The metal peak is also highly destabilized by more than 3 eVs. A metallic contribution is present in the lowest part of the DOS, which derives mainly from the non-metal network. The result of the interaction between the two sublattices leads to a shift of the Fermi levels down in energy by almost 2 eV, and an electron transfer from the anionic boron−carbon chains toward the cationic metal atoms (see Table 2). This electron transfer from B−B bonding and B−C antibonding states toward M−M bonding states contributes to weaken the B−B bonds and strengthen the B−C and M−M contacts.

As shown in Table 3, calculations carried out on an MBC slab with distorted boron−carbon chains give very similar results. The total DOS and the atomic projections, not shown here, are almost identical. The energy difference in favor of the distorted B/C chain is very weak (0.04 eV per unit cell,

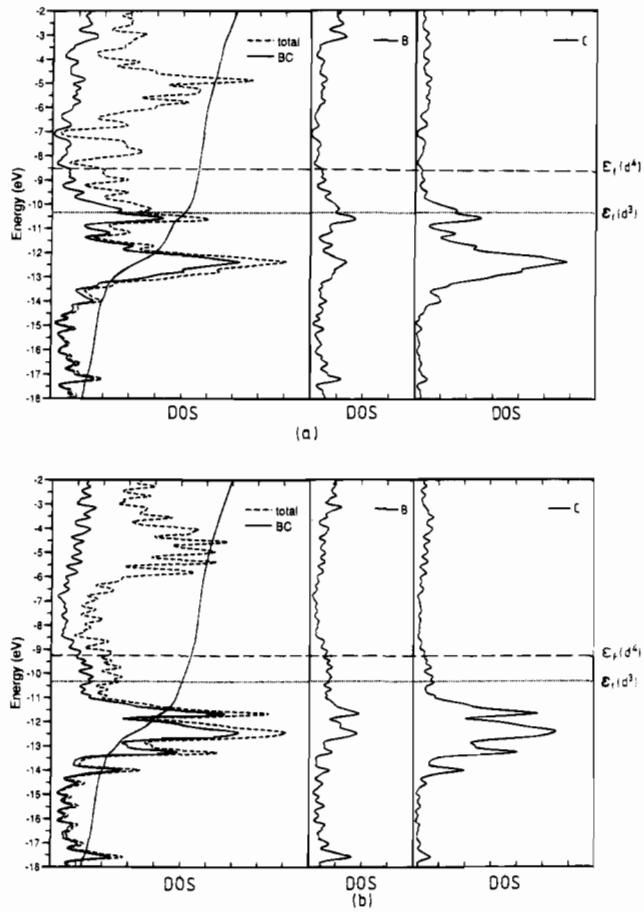

Figure 8. (a) Total DOS (dashed line), total boron + carbon contribution, boron contribution, and carbon contribution (solid line) for 3-D YBC. (b) Total DOS (dashed line), total boron + carbon contribution, boron contribution, and carbon contribution (solid line) for 3-D UBC. The Fermi level is indicated for a valence electron count of 3 (dotted line) and 4 (dashed line) per metal.

compare Tables 2 and 3). For the same reason as for the isolated $[(BC)^{4-}]_\infty$ model, the computed total energies do not reproduce strongly enough the preference for the MBC slab containing distorted B/C chains for the ThBC electron count (11 electrons per MBC). Some additional reason might arise from the fact that the two different slabs exhibit large sets of different M−B and B−B bond separations. It is known that EH calculations

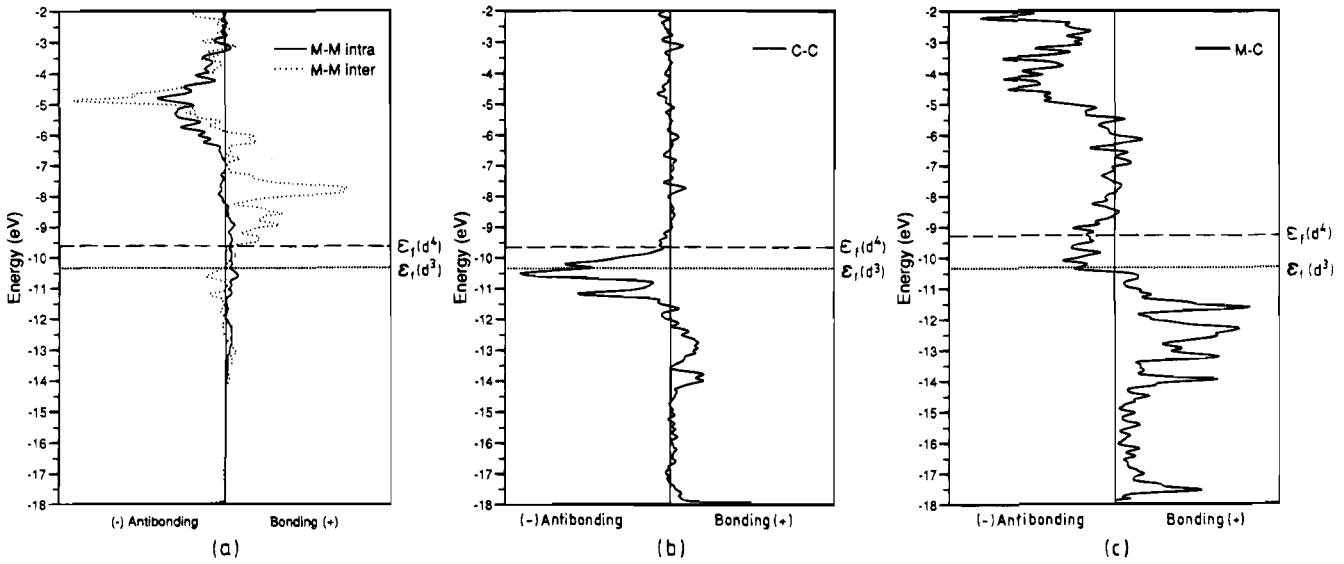

Figure 9. COOP curves for (a) intraslab M−M (solid line) and interslab M−M contacts (dotted line) in YBC. (b) Interslab C···C contacts in YBC. (c) Interslab M−C separations in UBC. The Fermi level is indicated for a valence electron count of 3 (dotted line) and 4 (dashed line) per metal.

do not accurately reflect the energy differences between structures with different and numerous atomic bond separations.[24]

(c) Three Different Ways of Stacking the MBC Slabs: The Full Structures of YBC, UBC, and ThBC. As mentioned earlier, the different ways of stacking the 2-D MBC slabs lead to three different structural types. In order to understand these different arrangements, calculations were performed on idealized 3-D structures corresponding to that of YBC, UBC, and ThBC (see the Appendix). The DOS of YBC and UBC[25] are given in Figure 8. They may be compared to that shown for an MBC slab illustrated in the middle of Figure 7. Only some tiny changes must be noted.

In YBC, the M−M interslab contacts induce additional M−M bonding and antibonding states in the DOS. Being mostly vacant regardless of the electron count (see Figures 8a and 9a), the very slightly negative M−M overlap populations that are computed (see Table 2) are not due to these states, but rather to some mixing of M−M antibonding states in the occupied boron−carbon band. The boron projected DOS in YBC is almost identical to that of the 2-D MBC slab. On the other hand, the carbon one is modified because of the C···C interslab contacts (2.50 Å). The peak of carbon DOS around −10.5 eV was not present in the 2-D MBC slab. As shown in Figure 9b, this peak which lies in the region of the Fermi level, is C−C antibonding and then responsible for the observed slight C−C repulsion (see Table 2). As a result, our calculations find such a stacking mode unstable vis-a-vis the isolated MBC slab. However, if the interslab separation is slightly shortened at 2.40 Å, calculations then indicate a positive C−C overlap population (0.021). This value increases to 0.164 at a C−C separation of 2.20 Å. Indeed, the C−C antibonding peak rises in energy when the C−C distances are shortened and its electrons are then poured into the bottom of the M−M bonding metallic band, strengthening somewhat the interslab M−M contacts. Although our calculations reproduce this interslab bonding at separations shorter than the experimental one, it is very likely that these weak covalent interactions are responsible for the stacking mode in YBC. Such an arrangement should be favored with rather electronegative metal elements exhibiting a low metallic d band, like yttrium. The fact that the C−C overlap populations are less strongly repulsive with 3 valence electrons per metal than with 4 renders unlikely such a stacking with Th or Ce.

According to our calculations the UBC structural type is strongly favored over the YBC one by 1.20 and 0.98 eV for 3 and 4 valence electrons per metal, respectively. This result, though overestimated somewhat, is in agreement with experiment which shows that YBC cleaves easily in the (101) planes and is more fragile than UBC. Moreover, the f-orbitals of U (not included in the calculations, see Appendix) might participate somewhat in U−C bonding and play in turn some role in the stacking preference of the MBC slabs in UBC compared to that of YBC. As we can see in Figure 8b, the M−C contacts linking the slabs in UBC modify slightly the DOS of the 2-D slab. We note a spreading and a small stabilization and destabilization of the boron−carbon and metallic bands, respectively, due to some interslab metal-carbon interactions. The interslab M−C overlap population is particularly strong whatever the metal valence electron count (3 or 4, see Table 2). However, it is slightly larger for the electron count of 3. It turns out that there is a peak of DOS which is somewhat interslab M−C antibonding around the Fermi levels (see Figure 9c). Occupying this peak weakens the M−C distances and consequently this type of arrangement. For 3 valence electrons per metal atom, short interslab M−C separations should be favored with the M−C antibonding peak remaining empty. On the other hand, long M−C contacts should be expected with 4 valence electrons per metal, rendering the occupied M−C peak less antibonding. This is indeed what is observed. Interslab M−C distances are shorter in UBC than in ThBC (*vide supra*). Calculations carried out on the ThBC structure show that the interslab M−C peak is now lowered in energy and fairly nonbonding. Both Fermi levels (for 3 and 4 metal valence electrons) are higher in energy crossing states having no interslab M−C contribution. The M−C overlap population is consequently the same for 3 and 4 valence electrons per metal. This is the major difference we note when the results of ThBC are compared to those of UBC.

Calculations were also performed on $Th_3B_2C_3$ using the experimental structure.[14] Relevant results are gathered in Table 3. An analytical detective work done on the different total and projected DOS and COOP curves computed for this material,

(24) See for example: Burdett, J. K.; Canadell, E. *Inorg. Chem.* **1988**, *27*, 4437.
(25) Lohr, L. L. *Int. J. Quantum Chem.: Quantum Chem. Symp.* **1991**, *25*, 121.

shows that the bonding mode of the ThBC sublattice present in $Th_3B_2C_3$ resembles that of the ThBC material.

Finally, let us mention that in all compounds that we studied, the Fermi levels computed either for 3 or 4 metal valence electrons cross the bottom of the metallic d band and the top of the B−B bonding band. Isotropic metallic behavior is expected for these types of materials. The metallic d-band being formally empty, the slight but nonnegligible metal−metal bonding present in those materials results mainly from through-bond interactions, due to some mixing of metal−metal bonding states in the occupied boron−carbon band.

Acknowledgment. Thanks are expressed to Professor J. K. Burdett for helpful discussions and L. Hubert for his expertise in the illustrations. F.W. is grateful to the Région Bretagne for financial support. P. R. thanks the Austrian Academy of Sciences for a research grant at the INSA, Rennes, France.

Appendix

All molecular and tight-binding calculations were carried out within the extended Hückel formalism[26] using standard atomic parameters for *B* and *C*. Different sets of parameters for the metal atoms were used. They led to basically the same qualitative conclusions, whatever the metal considered. Therefore, in order to facilitate the comparison between the different materials, we chose to present here the results obtained with the parameters of yttrium. The role of the rather contracted f orbitals for Th and U has been neglected, and they were thus not included in the calculations. The exponent (ζ) and the valence shell ionization potential (H_{ii} in eV) were, respectively, as follows: 1.3, −15.2 for B 2s; 1.3, −8.5 for B 2p; 1.625, −21.4 for C 2s; 1.625, −11.4 for C 2p; 1.39, −8.6 for Y 5s; 1.39, −5.0 for Y 5p. The H_{ii} for Y 4d was set equal to −8.4 eV. A linear combination of two Slater-type orbitals of exponents $\zeta_1 = 4.33$ and $\zeta_2 = 1.4$ with weighting coefficients $c_1 = 0.5827$ and $c_2 = 0.6772$ was used to represent the 4d atomic orbitals of Y.

In all models, B−C distances were set equal to 1.60 Å. B−B distances were 2.02 Å and 1.82/2.22 Å in the regular and distorded boron zigzag chains, respectively. Angles of 120° were taken around the boron atoms. MBC 2-D slabs were idealized with M−M distances of 3.50 Å. We have checked that calculations performed on the real slabs gave comparable results. For the 3-D models, an interslab separation of 2.50 Å was set for C···C in YBC, and 2.30 and 2.40 Å for M−C in UBC and ThBC, respectively. Calculations on idealized and experimental structures of YBC,[5] UBC,[10] ThBC[13] were compared. The experimental structure of $Th_3B_2C_3$[14] was used for the calculations.

For the calculations of the density of states, overlap populations and atomic net charges of the 1-D and 2-D models, sets of 51 and 64 *k* points were chosen in the irreducible Brillouin zone, respectively. For the 3-D materials, sets of 25, 25, 5, and 32 *k* points were taken in the irreducible wedge of the appropriate Brillouin zone of the YBC, UBC, ThBC, and $Th_3B_2C_3$, respectively. All *k* point sets were chosen in accordance with the geometrical method described by Ramirez and Böhm.[27]

IC9411357

(26) (a) Hoffmann, R. *J. Chem. Phys.* **1963**, *39*, 1397. (b) Whangbo, M.-H.; Hoffmann, R. *J. Am. Chem. Soc.* **1978**, *100*, 6093.

(27) Ramirez, R.; Böhm, M. C. *Int. J. Quantum Chem.* **1986**, *30*, 391.